

TIMo – A Dataset for Indoor Building Monitoring with a Time-of-Flight Camera

Pascal Schneider^{*}, Yuriy Anisimov^{*}, Raisul Islam^{*}, Bruno Mirbach^{*},
Jason Rambach^{*}, Frédéric Grandidier[†] and Didier Stricker^{*}

^{*} DFKI – German Research Center for Artificial Intelligence, firstname.lastname@dfki.de

[†] IEE S.A., Luxembourg, frederic.grandidier@iee.lu

Abstract

We present TIMo (*Time-of-flight Indoor Monitoring*), a dataset for video-based monitoring of indoor spaces captured using a time-of-flight (ToF) camera. The resulting depth videos feature people performing a set of different predefined actions, for which we provide detailed annotations. Person detection for people counting and anomaly detection are the two targeted applications. Most existing surveillance video datasets provide either grayscale or RGB videos. Depth information, on the other hand, is still a rarity in this class of datasets in spite of being popular and much more common in other research fields within computer vision. Our dataset addresses this gap in the landscape of surveillance video datasets. The recordings took place at two different locations with the ToF camera set up either in a top-down or a tilted perspective on the scene. The dataset is publicly available at <https://vizta-tof.kl.dfki.de/timo-dataset-overview/>.

1. Introduction

Traditionally, surveillance cameras are RGB or IR cameras. For the realization of robust automatic building management functions, time-of-flight depth cameras offer, however, some unique benefits. First of all they are more robust to illumination and color variations, and allow natural geometrical background removal. The depth information they provide allows to detect, classify and localize persons and objects precisely in 3D space. Moreover people are much less likely to be identifiable in depth data compared to RGB. Thus, monitoring places and at the same time preserving people’s privacy can be reconciled to a much better degree. For these reasons, the first building management systems based on time-of-flight technology have been around for about 10 years. (see ¹), which realize a small set

¹<https://www.iee-sensing.com/en/building-management-security.html>

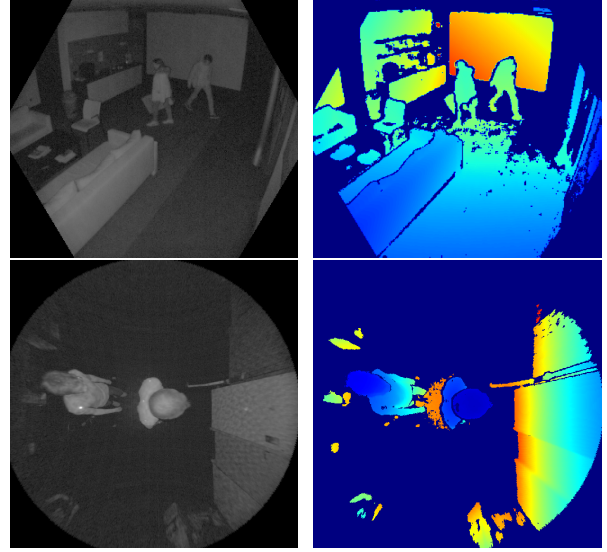


Figure 1: Example frames from our dataset. Top: a scene from tilted view, Bottom: a scene from top-down view. Left: IR image: Right depth image with depth encoded as color

of building management functions such as people counting or single access control. Future time-of-flight sensors with higher sensitivity and resolution in combination with novel deep-learning algorithms promise to both enhance the performance of existing building management systems and to realize novel functions as the behaviour analysis of persons and detection of anomalous situations.

The increasing affordability of consumer depth cameras has helped the analysis of depth data from time-of-flight sensors to become a popular and established part of current computer vision research. Examples of frequently used devices in this context are the *Microsoft Kinect* [22], *Intel RealSense* [8] or *Asus Xtion* [6]. The benefits of depth images to provide 3D geometric information has made it a

widely used data modality for certain applications such as action recognition [20] or gesture classification [19]. With our dataset we want to foster research towards robust and high performing person detection and novel smart building functions such as the detection of anomalies.

An advantage of our dataset over existing ones is the choice of more modern hardware. Our recordings were captured using a *Microsoft Azure Kinect* camera, which features higher image resolution, higher field-of-view and lower distance error compared to the *Microsoft Kinect v2*. [18, 21].

Some anomaly datasets additionally suffer from a very limited number of anomalous events. This is sometimes due to the fact that they use actual surveillance footage where anomalies tend to be rare. While there are advantages to using data from real-world anomalies, it can severely limit the amount of data available for testing anomaly detection algorithms. Our dataset features a large number of anomalies that facilitates testing at scale.

The rise of deep neural networks as the primary approach for solving computer vision problems leads to a demand for very large datasets that support training and testing complex models. Our dataset consists of about 1500 recordings with 44 different subjects and in total sums up to more than 612,000 individual video frames, which makes it suitable for the development of data-hungry approaches. Additionally, 243 sequences with 22,700 labeled frames with 3D bounding boxes and segmentation mask are provided for the person detection with counting purposes. It is moreover relatively easy to generate high quality synthetic data for depth videos in case the real data is not sufficient, since computation of depth is a customary step of computer graphics pipelines anyway. The *TiCAM* dataset is an example of how synthetic depth data can complement real data [7].

The rest of the paper is structured as follows: Sec. 2 puts our dataset into context w.r.t. existing ones. Sec. 3 then details the content and process of acquisition of our recordings and the accompanying annotations.

2. Related Work

The popularity of depth-sensing technology led to a large number of datasets to be released featuring RGB videos with an additional depth channel, or, in short, RGB-D. While pure RGB datasets can sometimes be compiled using existing recordings (such as videos on online video platforms), RGB-D data usually has to be recorded specifically for the dataset. A review of some of these datasets is given in [5]. Some provide static scans of indoor spaces, e.g. *Stanford 2D-3D-Semantics* [2] or *ScanNet* [4] and are commonly used for tasks such as semantic segmentation of point clouds.

Our dataset differs from this type of dataset in that it does not focus on the reconstruction of the static geometry of the indoor space but instead on capturing human action per-

formed within the scene. In this regard it is more similar to datasets used for action recognition such as *UTD-MHAD* [3] or *NTU RGB+D* [15] and *NTU RGB+D 120* [10]. However, these datasets were not created for the applications of anomaly detection or people counting. The camera angles and the nature of the recorded scenes make them unsuitable for these tasks. Therefore, there is a need for datasets particularly geared towards the development of algorithms for monitoring indoor spaces.

Existing datasets for anomaly detection usually provide only RGB data, e.g. the *Shanghai-Tech* dataset [11] or *UCF-Crime* [17]. Our dataset fills this existing gap by providing depth data of realistic scenarios and following camera angles as they would be common in a surveillance context.

Unlike some other datasets – such as [10] – we did not aim for a large variety of backgrounds or illumination in the data. This limitation is a consequence of the time-consuming process of calibration and the risk of having correlations between the background and the content of sequences, which has the potential to compromise the learning process and results when using machine learning. In addition, background variations are less relevant in depth data. We therefore committed to record only a few scenes and put more focus on a large and well balanced variance of subjects and actions and on providing high quality supplementary information, e.g. camera calibration parameters.

3. TIMo Dataset

We describe the content of the dataset as well as the process of recording. Sec. 3.2 and 3.3 cover the choice of hardware and scene and how recordings were carried out. Sec. 3.4 – 3.6 give more details about the content and annotations we provide in the dataset.

3.1. Data Modalities

We provide the infrared (IR) images and the depth maps estimated by the Microsoft Azure Kinect camera. The camera in principle also features recording RGB images, which we use in some of the figures for visualization purposes. Note, however, that our focus lies on depth data and hence we do not provide RGB frames in the public dataset and there are also no annotations for the RGB modality.

3.2. Setup

Recordings took place at two different locations, which we will refer to as *Scene 1* and *Scene 2*. *Scene 1* is an open office area with a small kitchen and a seating area. For this scene the Microsoft Azure Kinect camera was installed in two different positions. There was a tilted-view mounting in which the camera was able to monitor a large portion of the room including the four entrance possibilities, as shown in Fig. 3. In addition, the camera was mounted on a metal

Dataset	Year	# Sequences (# Frames)	Data Modalities	Camera Hardware	Annotations	Environ- ment
TIMo Anomaly Detection (ours)	2021	1588 (612K)	IR, Depth	MS Kinect Azure	Anomaly Frames	Indoor
TIMo Person Detection (ours)	2021	243 (23.6K)	IR, Depth	MS Kinect Azure	2D + 3D Object BBox, 2D Segm. Masks	Indoor
ShanghaiTech Campus [11]	2018	437 (317K)	RGB	RGB Camera	Anomaly Frames, Anomaly Masks	Outdoor
UTD-MHAD [3]	2015	861 (45K)	RGB, Depth, 3D Joints, ID	MS Kinect v1	Action Classes	Indoor
NTU-RGB+D 120 [10]	2019	114K (4M)	RGB, Depth, 3D Joints, Inertia	MS Kinect v2	Action Classes	Indoor
UCF-Crime [17]	2018	1900 (13.8M)	RGB	RGB Camera	Anomaly Frames	Indoor + Outdoor
TiCAM (Real) [7]	2021	533 (6.7K / 118K)	RGB, IR, Depth	MS Kinect Azure	2D + 3D Object BBox, 2D Segm. Masks / Action Classes	Car Cabin
DAD [9]	2020	386 (2.1M)	IR, Depth	CamBoard pico flexx	Anomaly Frames	Car Cabin
CUHK Avenue [12]	2013	37 (31K)	RGB	RGB Camera	Anomaly Frames, Anomaly BBoxes	Outdoor
UCSD Ped 1 + 2 [13]	2010	70 + 28 (14K + 4.6K)	Greyscale	Greyscale Camera	Anomaly Frames, Anomaly Masks ²	Outdoor
Subway Exit + Entrance [1]	2008	1 + 1 (137K + 72K)	Greyscale	Greyscale Camera	Anomaly Frames, rough Anomaly Location	Subway Station
IITB-Corridor [14]	2020	368 (484K)	RGB	RGB Camera	Anomaly Frames	Outdoor (Corridor)

Table 1: Comparison of related datasets to our dataset. 3D joints refers to joints of the human body such as the are used in pose estimation.

frame above the entrance B with a top-down view, monitoring people entering or leaving the room through a hallway.

The same top-down mounting orientation has been used in *Scene 2* but with more flexibility. There the monitored area is less confined, allowing persons to cross the scene in all directions. Moreover, the camera is mounted on a lift allowing to vary the camera height. Fig. 2 shows the different camera mounting setups. For the two different mounting orientations, the camera configuration was different as described below.

3.2.1 Top-down View

For top-down recordings we used the wide field-of-view (WFOV) configuration of the Azure Kinect ($120^\circ \times 120^\circ$). The native resolution of the sensor in WFOV configuration is 1024×1024 pixels. We employ a 2×2 binning technique which reduces the resolution down to 512×512 pixels but at the same time yields a higher operating range, which is 0.25 m – 2.88 m. The capturing rate is set to 30 frames per second (FPS). The camera height above ground

was varied between 2.25 m, 2.50 m and 2.75 m

3.2.2 Tilted-view

For recordings from the tilted view we used the narrow field-of-view (NFOV) configuration ($75^\circ \times 65^\circ$). The native resolution of the sensor in NFOV configuration is 576×640 pixels. Same as for the top-down configuration, we use a frame rate of 30 FPS and 2×2 binning, which results in a resolution of 288×320 pixels.

The maximum guaranteed depth operating range for the NFOV configuration with 2×2 binning is 5.46 m. For the recordings from the tilted-view camera this is not enough range to cover the complete scene. As is usual for time-of-flight cameras, the data quality also depends significantly on the remission properties of the surface in question. Nevertheless we observed that we get adequate depth measurements for the relevant parts of the scene up to about 10 m in our setup.



(a) Camera mounting for tilted-view scene. (b) Setup for top-down view in *Scene 1*. (c) Setup for top-down view in *Scene 2*.

Figure 2: Recording setups used for capturing the dataset.

3.3. Acquisition

The test cases were defined prior to recording according to a test matrix, which aims at preventing unintentionally introduced correlations in the dataset. The anomalies in the anomaly dataset also belong to pre-defined test cases. The camera was calibrated according to a world coordinate system before each recording session. For recording, the test subjects were instructed to enter and leave the scene through a specific entrance. For the tilted-view scene there are four such entrances (see Fig. 3). In the top-down-view scenes the test subjects cross the scene either in the X – or Y – direction of the camera coordinate system. The subjects perform a given action after entering the scene and then leave again. The instructions on how an action was to be performed were kept rather vague in order to have some degree of variance between performances of the same action type. A full list of the choreographies can be found on the dataset website³.

³<https://vizta-tof.kl.dfki.de/building-data-format/>

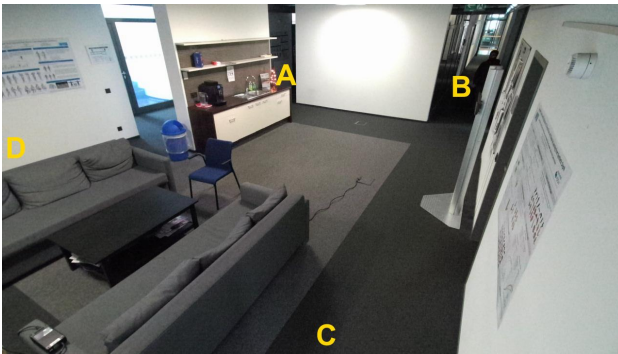


Figure 3: Tilted-view scene with marked entrances.

3.4. Post-Processing

Post-processing of the data and the annotations is kept to a minimum in order to allow users to choose between using the raw data or applying custom normalization themselves. Images in the person detection dataset are undistorted and remapped to the common pinhole camera model. The original rotation and translation matrices are also provided per sequence for its further conversion to the 3D world coordinate system (e.g. in a form of a point cloud). The segmentation masks and 2D bounding boxes are provided in the coordinates of the undistorted and remapped images (see Sec. 3.6 for more details on the annotations).

3.5. Data Format

The IR and depth videos are stored as individual frames in the *Portable Network Graphics* (PNG) format with a single 16-bit channel. The pixel values in the depth images directly correspond to the depth measurements in millimeters. A pixel value of 0 is used as a special value to indicate that there is no valid depth estimation for this pixel. Note that the example frames shown in this paper have been transformed w.r.t. value range and contrast for better visualization.

The video sequences and individual frames follow a common naming scheme which includes the most relevant information directly in the file name. It includes the choreography, a sequence ID, the camera height, a timestamp and a calibration ID. More details on the naming scheme can also be found on the website³.

3.6. Annotations

We provide annotations for people and objects in the form of 2D and 3D bounding boxes and segmentation masks for the person detection dataset and anomaly annotations for the anomaly dataset. For the anomaly dataset both tilted view data recorded in *Scene 1* and top-down data recorded in *Scene 2* were annotated. For the person detec-

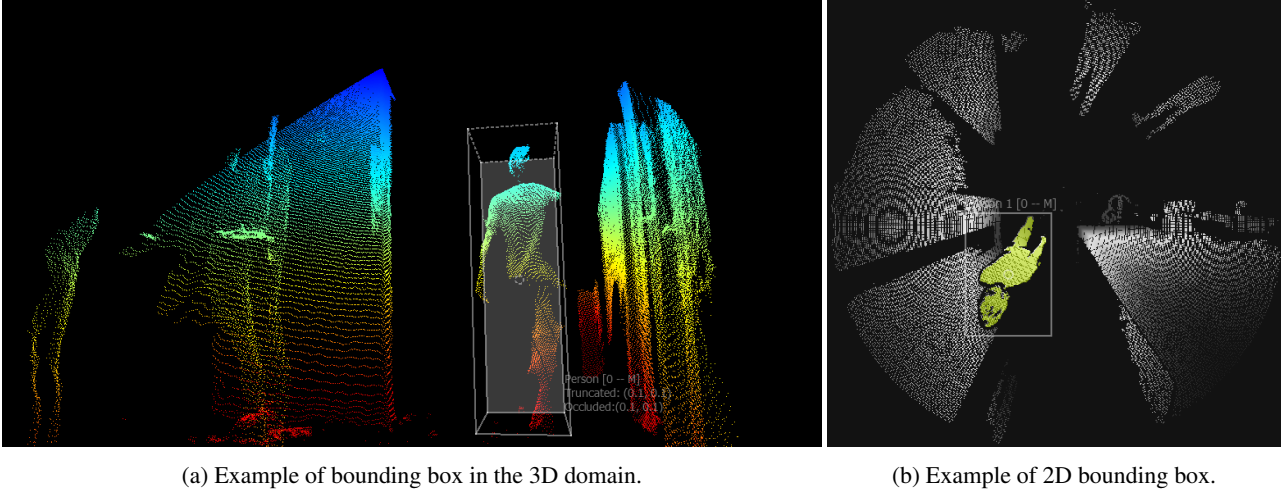


Figure 4: Visualization of annotations for the person detection/people counting dataset, generated by [16].

tion dataset data from both scenes recorded in the top-down configuration were annotated. The annotations were done manually using a software tool that was developed specifically for the purpose of annotating 3D data [16].

3.6.1 Anomaly Annotations

Anomaly annotations are provided as pairs of frame indices which indicate when the anomalous event within the given sequence starts and ends. Note that the frames at `START_FRAME_IDX` and `END_FRAME_IDX` both also belong to the anomalous event, thus making it `END_FRAME_IDX - START_FRAME_IDX + 1` frames long.

Examples of anomalies include left behind objects, people arguing or throwing objects. Fig. 5 illustrates two instances of anomalous events within the dataset.

All choreographies that are not labeled as anomalous are consequently considered to be normal. This includes activities such as getting coffee from the kitchen, talking with one another or simply walking.

3.6.2 Person and Object Annotations

For the person detection we provide annotations for people and objects in the following form:

- 2D segmentation masks per frame, saved as 8-bit PNG images. Pixel values correspond to class and instance IDs respectively;
- 2D bounding boxes per annotation, described as pixel coordinates of rectangular around the annotated object. This data is presented in corresponding CSV in a form of $[x_1, y_1, x_2, y_2]$, where (x_1, y_1) and (x_2, y_2) are the start and end coordinates of the bounding box;

- 3D bounding boxes per annotation, presented in corresponding CSV as a box center (cx, cy, cz) and its dimensions (dx, dy, dz) in the world coordinate system.

Objects are annotated as a separated class only if they are not held by a person at the specific frame. The 3D bounding boxes are generated automatically using the segmentation masks, since the calibration of the camera allows a direct mapping between the 2D image space and the 3D point clouds implicitly given in the form of the depth maps. We also used interpolation between manual annotations to speed up the process in situations where this could be done without impairing the quality of the annotations. All annotations were additionally validated by a person different from the one who created the annotation.

Examples of these annotations are illustrated in Fig. 4.

Person Detection Dataset			
Data Type	Sequences	Frames	Annotations
Training	125	6,415	8,501
Complex Training	34	7,675	8,186
Total	159	14,090	16,687
Testing	72	5,089	6,129
Complex Testing	12	3,533	4,971
Total	84	8,622	11,000

Table 2: Data statistics of the person detection dataset.

3.7. Data Statistics

Tab. 3 and Tab. 2 show the splits of datasets in training and testing data. For the case of person detection, there are

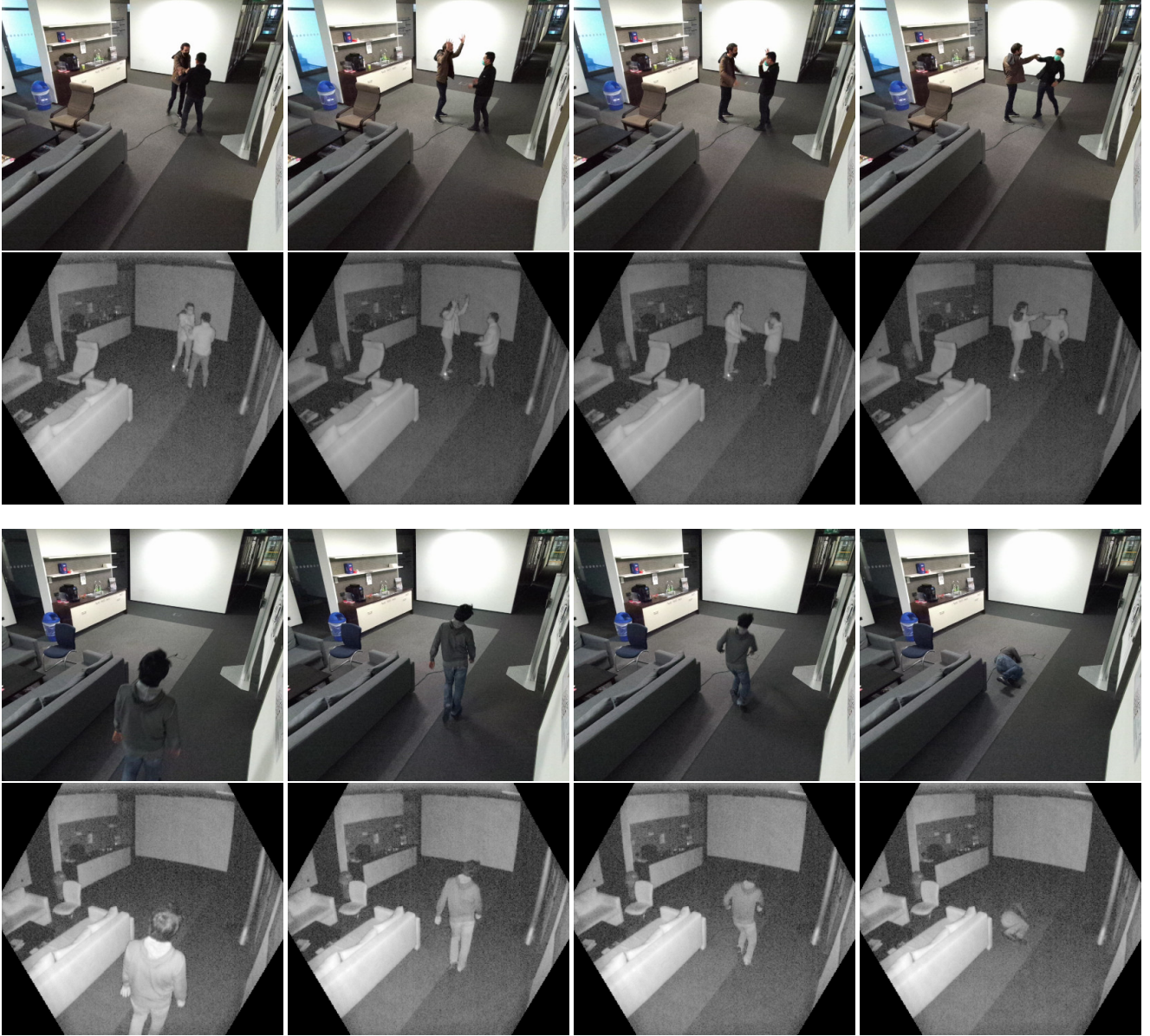


Figure 5: Examples of anomalies. The top row shows frames from a sequence with an argument (CROSS_ARG) between two people, the bottom row a collapsing person (COLLAPSE).

approximately 14K frames from 159 sequences for training and 8.6K frames from 84 sequences for testing. Both the training and testing set have been further split according to the complexity of the scenes. *Scene 2* data were recorded with a camera mounted at different heights, also in this scene the variety of movements is greater than in *Scene 1*, which explains the choice of these sequences for training. In contrast, data from *Scene 1* captured with the camera mounted at 2.50 m and suggested to be used for testing. Complex top-down sequences were captured at *Scene*

2 and split to training and testing sets based on the captured person and his activity.

The anomaly dataset consists in total of 929 sequences for training and 659 sequences for testing. The data splits are designed for usage with unsupervised learning techniques. Therefore the training set only consists of normal sequences. The test set mostly consists of sequences that contain anomalies, but also contains some normal sequences as well. Also including normal sequences in the test split aims at facilitating the evaluation of the false pos-

Anomaly Dataset – Train Split								
Configuration	# Sequences			# Frames			Unique Choreographies	
	Normal	Anomalous	Total	Normal	Anomalous	Total	Normal	Anomalous
Tilted View	285	0	285	185,620	0	185,620	31	0
Top-down View	624	0	624	180,359	0	180,359	19	0
Total	909	0	909	365,979	0	365,979	36	0

Anomaly Dataset – Test Split								
Configuration	# Sequences			# Frames			Unique Choreographies	
	Normal	Anomalous	Total	Normal	Anomalous	Total	Normal	Anomalous
Tilted View	31	151	182	66,508	25,617	92,125	29	20
Top-down View	79	418	497	104,165	49,528	153,693	18	12
Total	110	569	679	170,673	75,145	245,818	34	22

Table 3: Data statistics of the anomaly dataset’s train and test split. The train split does not contain anomalies since the split was made for usage with unsupervised methods. Note that there some choreographies are used in both the tilted- as well as the top-down view, so the total number of unique choreographies is less than the sum from the configurations.

itive rate. Because of the two different camera configurations, used in the recordings in *Scene 1*, both training and test set are split accordingly.

4. Conclusion

We presented an extensive dataset of video sequences for monitoring indoor scenes consisting of IR and depth videos captured by a time-of-flight camera of the latest generation. It consists of about 1500 sequences for the anomaly detection use case and about 240 sequences for the person detection and people counting use case. We described the data and the associated annotations as well as the recording setup and process. The dataset aims at facilitating the development of depth-based algorithms for monitoring indoor spaces in order to allow such functionality to be implemented in a more privacy-preserving way.

Acknowledgements

This work was partially funded within the *Electronic Components and Systems for European Leadership* (ECSEL) joint undertaking in collaboration with the European Union’s *H2020 Framework Program* and the *Federal Ministry of Education and Research* of the Federal Republic of Germany (BMBF), under grant agreement 16ESE0424 / GA826600 (VIZTA).

Special thanks to the researchers at DFKI and IEE who contributed to the planning and recording of the dataset: Hartmut Feld, Ibrahim Abdelaziz, Dennis Stumpf, Jigyasa Singh Katrolia, Alain Garand, Frederic Garcia, Valeria Serchi, Thomas Solignac. We would also like to thank the students who worked on annotating the data: Sai Srinivas Jeevanandam, Ahmed Elsherif, Brijesh Varsani and Kannan Balakrishnan.

References

- [1] Amit Adam, Ehud Rivlin, Ilan Shimshoni, and David Reinitz. Robust real-time unusual event detection using multiple fixed-location monitors. *IEEE Trans. Pattern Anal. Mach. Intell.*, 30(3):555–560, 2008. 3
- [2] I. Armeni, A. Sax, A. R. Zamir, and S. Savarese. Joint 2D-3D-Semantic data for indoor scene understanding. *ArXiv e-prints*, Feb. 2017. 2
- [3] Chen Chen, Roozbeh Jafari, and Nasser Kehtarnavaz. UTD-MHAD: A multimodal dataset for human action recognition utilizing a depth camera and a wearable inertial sensor. In *2015 IEEE International Conference on Image Processing, ICIP 2015, Quebec City, QC, Canada, September 27-30, 2015*, pages 168–172. IEEE, 2015. 2, 3
- [4] Angela Dai, Angel X. Chang, Manolis Savva, Maciej Halber, Thomas A. Funkhouser, and Matthias Nießner. ScanNet: Richly-annotated 3D reconstructions of indoor scenes. In *2017 IEEE Conference on Computer Vision and Pattern Recognition, CVPR 2017, Honolulu, HI, USA, July 21-26, 2017*, pages 2432–2443. IEEE Computer Society, 2017. 2
- [5] Michael Firman. RGBD datasets: Past, present and future. In *2016 IEEE Conference on Computer Vision and Pattern Recognition Workshops, CVPR Workshops 2016, Las Vegas, NV, USA, June 26 - July 1, 2016*, pages 661–673. IEEE Computer Society, 2016. 2
- [6] Higinio Gonzalez-Jorge, Belén Riveiro, Esteban Vazquez-Fernandez, Joaquín Martínez-Sánchez, and Pedro Arias. Metrological evaluation of Microsoft Kinect and Asus Xtion sensors. *Measurement*, 46(6):1800–1806, 2013. 1
- [7] Jigyasa Singh Katrolia, Bruno Mirbach, Ahmed El-Sherif, Hartmut Feld, Jason Rambach, and Didier Stricker. TiCaM: A Time-of-flight In-car Cabin Monitoring Dataset, 2021. 2, 3
- [8] Leonid Keselman, John Iselin Woodfill, Anders Grunnet-Jepsen, and Achintya Bhowmik. Intel(R) RealSense(TM) stereoscopic depth cameras. In *2017 IEEE Conference on*

- Computer Vision and Pattern Recognition Workshops, CVPR Workshops 2017, Honolulu, HI, USA, July 21-26, 2017*, pages 1267–1276. IEEE Computer Society, 2017. 1
- [9] Okan Köpüklü, Jiapeng Zheng, Hang Xu, and Gerhard Rigoll. Driver anomaly detection: A dataset and contrastive learning approach. In *IEEE Winter Conference on Applications of Computer Vision, WACV 2021, Waikoloa, HI, USA, January 3-8, 2021*, pages 91–100. IEEE, 2021. 3
- [10] Jun Liu, Amir Shahroudy, Mauricio Perez, Gang Wang, Ling-Yu Duan, and Alex C. Kot. NTU RGB+D 120: A large-scale benchmark for 3D human activity understanding. *IEEE Trans. Pattern Anal. Mach. Intell.*, 42(10):2684–2701, 2020. 2, 3
- [11] Wen Liu, Weixin Luo, Dongze Lian, and Shenghua Gao. Future frame prediction for anomaly detection - A new baseline. In *2018 IEEE Conference on Computer Vision and Pattern Recognition, CVPR 2018, Salt Lake City, UT, USA, June 18-22, 2018*, pages 6536–6545. IEEE Computer Society, 2018. 2, 3
- [12] Cewu Lu, Jianping Shi, and Jiaya Jia. Abnormal event detection at 150 FPS in MATLAB. In *IEEE International Conference on Computer Vision, ICCV 2013, Sydney, Australia, December 1-8, 2013*, pages 2720–2727. IEEE Computer Society, 2013. 3
- [13] Vijay Mahadevan, Weixin Li, Viral Bhalodia, and Nuno Vasconcelos. Anomaly detection in crowded scenes. In *The Twenty-Third IEEE Conference on Computer Vision and Pattern Recognition, CVPR 2010, San Francisco, CA, USA, 13-18 June 2010*, pages 1975–1981. IEEE Computer Society, 2010. 3
- [14] Royston Rodrigues, Neha Bhargava, Rajbabu Velmurugan, and Subhasis Chaudhuri. Multi-timescale trajectory prediction for abnormal human activity detection. In *IEEE Winter Conference on Applications of Computer Vision, WACV 2020, Snowmass Village, CO, USA, March 1-5, 2020*, pages 2615–2623. IEEE, 2020. 3
- [15] Amir Shahroudy, Jun Liu, Tian-Tsong Ng, and Gang Wang. NTU RGB+D: A large scale dataset for 3d human activity analysis. In *2016 IEEE Conference on Computer Vision and Pattern Recognition, CVPR 2016, Las Vegas, NV, USA, June 27-30, 2016*, pages 1010–1019. IEEE Computer Society, 2016. 2
- [16] Dennis Stumpf, Stephan Krauß, Gerd Reis, Oliver Wasenmüller, and Didier Stricker. SALT: A semi-automatic labeling tool for RGB-D video sequences. In Giovanni Maria Farinella, Petia Radeva, José Braz, and Kadi Bouatouch, editors, *Proceedings of the 16th International Joint Conference on Computer Vision, Imaging and Computer Graphics Theory and Applications, VISIGRAPP 2021, Volume 4: VISAPP, Online Streaming, February 8-10, 2021*, pages 595–603. SCITEPRESS, 2021. 5
- [17] Waqas Sultani, Chen Chen, and Mubarak Shah. Real-world anomaly detection in surveillance videos. In *2018 IEEE Conference on Computer Vision and Pattern Recognition, CVPR 2018, Salt Lake City, UT, USA, June 18-22, 2018*, pages 6479–6488. IEEE Computer Society, 2018. 2, 3
- [18] Michal Tölgyessy, Martin Dekan, L’uboš Chovanec, and Peter Hubinský. Evaluation of the Azure Kinect and its comparison to Kinect v1 and Kinect v2. *Sensors*, 21(2):413, 2021. 2
- [19] Pichao Wang, Wanqing Li, Song Liu, Zhimin Gao, Chang Tang, and Philip Ogunbona. Large-scale isolated gesture recognition using convolutional neural networks. In *2016 23rd International Conference on Pattern Recognition (ICPR)*, pages 7–12. IEEE, 2016. 2
- [20] Pichao Wang, Wanqing Li, Philip Ogunbona, Jun Wan, and Sergio Escalera. RGB-D-based human motion recognition with deep learning: A survey. *Comput. Vis. Image Underst.*, 171:118–139, 2018. 2
- [21] Oliver Wasenmüller and Didier Stricker. Comparison of Kinect v1 and v2 depth images in terms of accuracy and precision. In Chu-Song Chen, Jiwen Lu, and Kai-Kuang Ma, editors, *Computer Vision - ACCV 2016 Workshops - ACCV 2016 International Workshops, Taipei, Taiwan, November 20-24, 2016, Revised Selected Papers, Part II*, volume 10117 of *Lecture Notes in Computer Science*, pages 34–45. Springer, 2016. 2
- [22] Zhengyou Zhang. Microsoft Kinect sensor and its effect. *IEEE Multim.*, 19(2):4–10, 2012. 1